PROCEEDINGS OF SPIE

SPIEDigitalLibrary.org/conference-proceedings-of-spie

Manufacturing and integration status of the UH2.2 adaptive secondary mirror

Wouter Jonker, Stefan Kuiper, Fred Kamphues, Arjo Bos, Bert Dekker, et al.

Wouter Jonker, Stefan Kuiper, Fred Kamphues, Arjo Bos, Bert Dekker, Mark Chun, André Benschop, Hans Priem, Bert Monna, Manav Nair, Taavishe Gupta, Gilles Ackaert, Suman Bola, Loannis Varvaringos, Julian Schroth, "Manufacturing and integration status of the UH2.2 adaptive secondary mirror," Proc. SPIE 12188, Advances in Optical and Mechanical Technologies for Telescopes and Instrumentation V, 1218816 (29 August 2022); doi: 10.1117/12.2629254



Event: SPIE Astronomical Telescopes + Instrumentation, 2022, Montréal, Québec, Canada

Manufacturing and Integration status of the UH2.2 Adaptive Secondary Mirror

Wouter Jonker^a, Stefan Kuiper^a, Fred Kamphues^a, Arjo Bos^a, Bert Dekker^a, Mark Chun^b, Andre Benschop^c, Hans Priem^c, Bert Monna^d, Manav Nair^d, Taavishe Gupta^d, Gilles Ackaert^d, Suman Bola^d, Ioannis Varvaringos^d, Julian Schroth^d

^aTNO Space&Scientific Instrumentation, Delft, the Netherlands; ^bUniversity of Hawaii, Institute for Astronomy, Hilo, USA; ^cVDL Enabling Technologies Group, Eindhoven, the Netherlands; ^dAAC Hyperion, Delft, the Netherlands

ABSTRACT

A consortium of industrial and academic partners, coordinated by TNO, is working on the realization of a 620mm adaptive secondary mirror (ASM) for the University of Hawaii's 2.2-meter telescope [1][2][3]. The ASM consists of a 620mm-diameter slumped convex aspherical mirror shell, manipulated by 210 variable-reluctance actuators mounted on a light-weighted support frame. The mirror shell is manufactured to the required accuracy at low cost through slumping. The actuators are driven by dedicated PWM current drivers and commanded through a real-time FPGA-based interface. After successful performance testing of several laboratory prototypes[4], this project will provide the definitive on-sky demonstration of this new technology. We report on the manufacturing and testing of the major subsystems, and on the integration status of the ASM as a whole.

Keywords: reluctance actuator, adaptive mirror, UH88, UH2.2, ASM

INTEGRATION STRATEGY

The planned high-level integration strategy is shown in the figure below. The order of integration determines some aspects of the detailed design as well as the manufacturing flow. The mirror shell is the single long-lead item and is needed first. The actuators have a medium lead time, while the support structure and the electronics can be manufactured fairly quickly.



Figure 1: integration sequence

A dedicated integration rig (Figure 2) is the basis with all required references and functionality for positioning the ASM parts. Integration will start with the lateral positioning of the facesheet on the rig. The precise centering of the facesheet is important since it's an asphere. The facesheet is placed on 18 support points (Figure 3) which can be adjusted to tune the initial shape of the facesheet. The initial shape is measured by placing the rig under a CMM and measuring at these 18 points after which the supports are re-adjusted if necessary. This process can be repeated until the facesheet is close enough to its final shape.

Advances in Optical and Mechanical Technologies for Telescopes and Instrumentation V, edited by Ramón Navarro, Roland Geyl, Proc. of SPIE Vol. 12188, 1218816 © 2022 SPIE · 0277-786X · doi: 10.1117/12.2629254



Figure 2: ASM integration rig built by West End

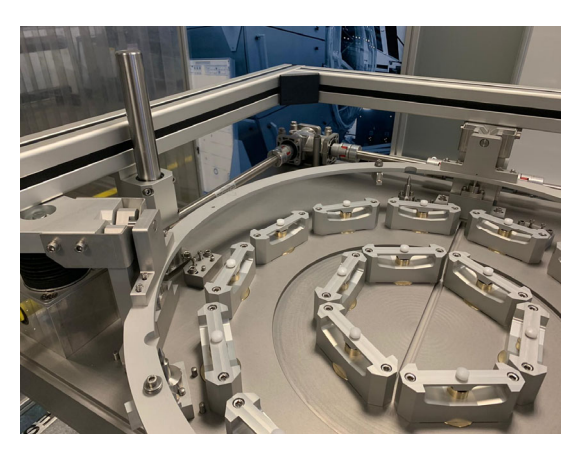


Figure 3: detailed view of the facesheet positioners

The next step in integration will be placing the mechanical support structure. With a hoisting tool the structure is lowered onto guiding rods, and brought to the proper distance from the facesheet. Next, the puck and strut, which will form the mechanical connection from facesheet to actuator, are bonded. Lateral movement of the facesheet is constrained by a two-piece Titanium alloy lateral support located in the center of the structure. The CTE of the Titanium matches the CTE of the glass, minimizing print-through at the bonded flexures. After this, the actuators are mounted on the back of the support structure and bonded to the struts. The electronics are installed after complete end-to-end testing offline. Integration will finish with the installation of dust seals and protective covers. With the above strategy in mind, the final design details of the strut, puck and lateral support were finished and procurement of parts was launched. The manufacturing of the facesheet is described in a separate publication [5].

ACTUATORS

The heart of the UH2.2-ASM lies in its in-house developed hybrid variable reluctance actuators, which have a high efficiency in terms of force per unit volume and per unit power [1]. The performance of the actuators in combination with a representative facesheet thickness has been thoroughly tested by UCSC with the 19-actuator FLASH DM [4]. At the core of the magnetic circuit, these actuator generate a linear force range of $\pm 8N$ (99% linearity). Using an internal lever-arm this force gets amplified to a force-range of $\pm 22N$ and a displacement of $\pm 20\mu m$ at the strut interface to the facesheet. The first mechanical resonance of 1,2kHz is sufficient to reach the targeted closed-loop disturbance rejection bandwidth of 100Hz. During normal operation the power dissipation of these actuators is only a few mW per actuator, which negates the need for active cooling. Additional provisions are integrated to enable the replacement of an actuator in case this is needed.

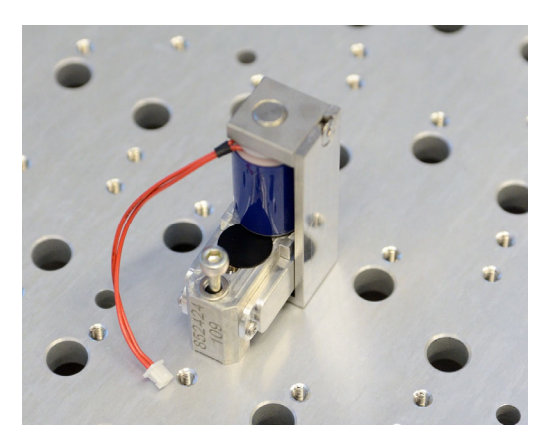


Figure 4: ASM actuator with coil integrated



Figure 5: Actuator mounted in functional testing jig

After successful testing of FLASH, the full set of 210 actuators plus spares was manufactured, assembled and functionally tested by VDL-ETG. Using a dedicated test-rig shown in Figure 5, all actuators have undergone acceptance testing where the displacement range was measured using a microprobe.

STRUCTURE AND BONDING

The actuators are mounted on a rigid support structure, consisting of two Aluminum light-weighted Ø630mm half-shells[1]. This support structure provides stability and rigidity for the overall system during its dynamic operation. The first natural frequency of the assembled structure is >500 Hz, allowing an actuator control bandwidth of >100 Hz[3]. The support structure is attached to the triangular telescope interface with three quadropods, with its center of rotation close to center of gravity of the ASM. Compared to the original A-frame support design, there is less deformation and vertical displacement in the first mode, due to the reduced stiffness of the support. The lowest natural frequency of the ASM assembly on the telescope interface are two lateral modes at 170 Hz while a piston mode occurs at 287 Hz.

The structure parts were manufactured using 5-axis machining and inspected by CMM (Figure 6), before the application of a Surtec 850 surface treatment, to protect the Aluminum parts against corrosion. The two structural halves are bolted together with 141 stainless steel A4-80 electropolished and kolsterized Jeclin M4 fasteners. Together with the Nitronic 60 inserts in the structure, the kolsterizing treatment protects the fasteners from galling. The electropolishing treatment provides the fasteners with an extremely smooth surface, resulting in lower and more predictable friction, which, in turn, leads to excellent preload control during torquing.







Figure 7: Structure fit check in ASM assembly tool

The ASM lateral support is composed of two Titanium alloy parts, which are epoxy bonded to the glass and structure (Figure 8, Figure 9). Special tooling was developed to properly center and preload the components during the various stages of bonding.

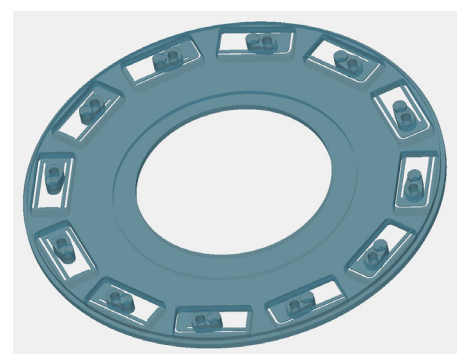


Figure 8: Lateral Support CAD model



Figure 9: Lateral Support Thermal Springs Ring

The connection between the 210 actuators and facesheet is made with bonded struts and pucks. The struts are stiff in the axial direction and compliant in the radial direction to minimize thermal distortions in the facesheet. The struts are all oriented perpendicular to the optical axis, and are connected to the facesheet via a puck. The puck has a spherical seat and enables a connection between 0° (center of face sheet) and 4° (edge of face sheet). A cross section of the ASM and strut to glass connections is shown in Figure 10.

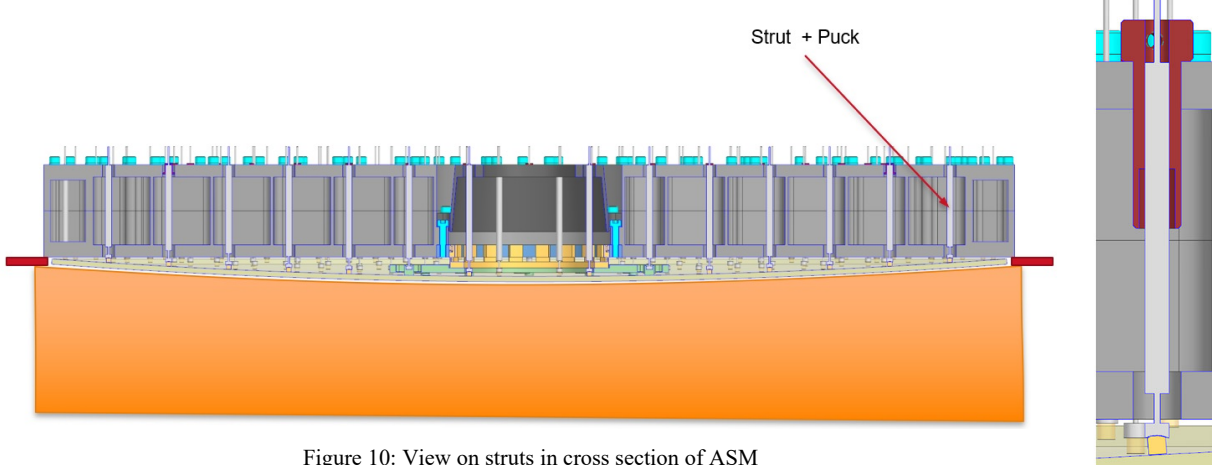


Figure 10: View on struts in cross section of ASM

High reliability and low maintenance are essential during operational conditions. With limited access to the struts and pucks after integration of the ASM, the reliability of the epoxy bonds between the struts and pucks and between the pucks and the facesheet must be very high. A high margin of strength w.r.t. the operational loads is required (ideally >>5). A low variation on the measured average bond strength indicates a stable process. In order to achieve these important requirements, the bonding process was optimized and verified extensively. Several setups were built to perform pull tests on bonded struts (Figure 11). The resulting average strut and puck axial bond strength is 299 N (31 MPa), with a standard deviation of 35N (Figure 13). All bond samples showed a cohesive fracture of the adhesive (Figure 12), indicating that the limit of the adhesive strength has been approached. The operational strut loads are maximum 20 N. A safety factor of 9.7 w.r.t. the measured 3σ strength value is considered more than adequate.

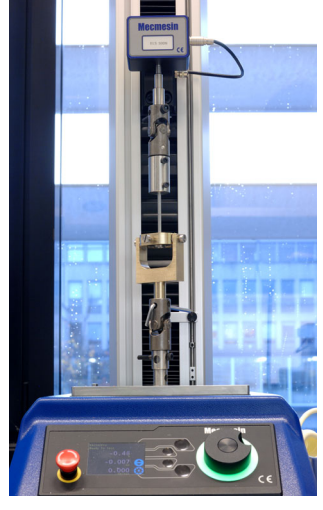


Figure 11: Bond pull testing

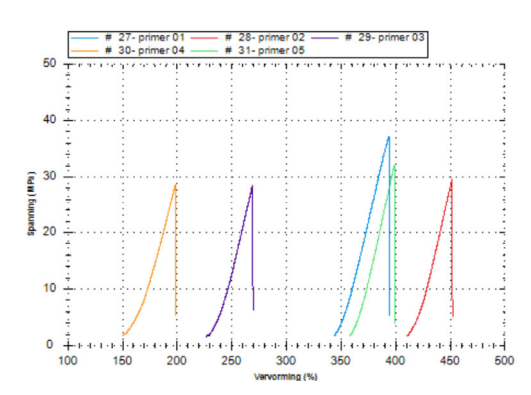


Figure 12: Axial tensile test results showing an average yield stress of around 31 MPa



Figure 13: Cohesive failure in adhesive bond

ELECTRONICS

A functional block diagram of is shown in Figure 14 below. Functions are distributed over separate PCB's which are mounted in an electronics box. This box is then mounted at the telescope spider structure in the shadow of the M2.

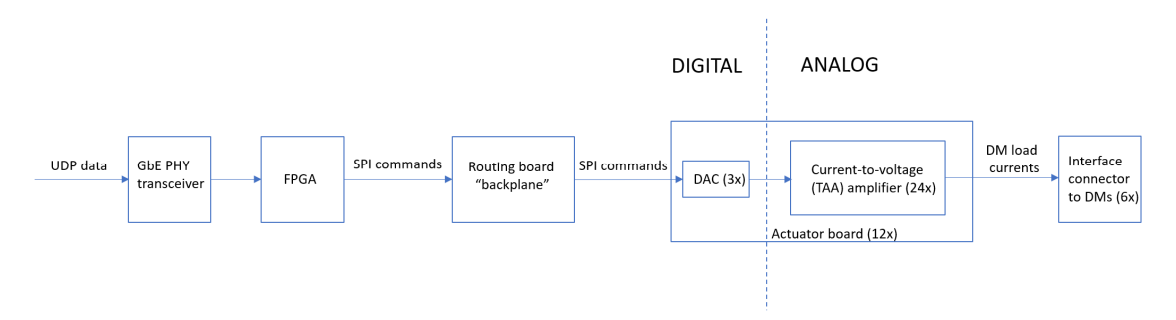


Figure 14: Electronics functional block diagram

The PHY transceiver – FPGA stack decodes the incoming UDP packets to multiple parallel SPI paths. The backplane distributes the signals to 12 separate actuator boards, each containing 24 channels. On these amplifier boards, the incoming SPI-signals containing the current setpoints are routed to the DACs and trans-admittance amplifiers (TAA) which generate the output currents. The current signals are routed to the distribution PCBs on the backside of the ASM through a cable harness. Figure 15 shows the backplane, FPGA and one actuator board mounted in the electronics box.



Figure 15: Electronics box - the long PCB on the bottom is the backplane, the standing PCB is one actuator board

Figure 16 shows one of the 12 actuator boards, with the L-C circuits that low-pass filter the PWM signals clearly visible. The design of this amplifier is critical to meeting the performance requirements including high current output capability in the range of several 100s of mA, sufficient bandwidth (2 kHz), high power efficiency, low spectral noise density over the entire bandwidth (below 10µA total integrated rms), low offset output current and good accuracy.

All electronics is tested thoroughly for functionality and performance. A prototype actuator board was tested for performance, including verification of the gain, steering range, accuracy, voltage-to-current frequency transfer function, power consumption and current noise spectral density.





Figure 16: Actuator board with 24 current amplifiers

Figure 17: Setup for end-to-end electronics testing

After successful testing the full set was released for manufacturing. All individual boards are then functionally tested. This includes e.g. continuity tests of the routing board/backplane; feeding generated test stimuli (UDP packets) into the FPGA and verifying the outputs (SPI data packets) with a hardware logic analyzer; and testing the actuator boards by providing readily generated SPI inputs to the DACs and measuring the corresponding current through a dummy load. Tests are repeated after connecting the boards together. Figure 17 shows the test setup, where a sinusoidal current is commanded through UDP and is also measured over the dummy load at the actuator board output.

The normalised small-signal magnitude frequency response of a single amplifier is shown in Figure 18. The bandwidth is around 2 kHz, which is sufficient for AO closed control loop control. The output noise current spectral density remains below the requirement for nearly all frequencies (Figure 19). The standard deviation of the noise after integration over a 50 kHz band (i.e. far above the control bandwidth) stays well below the required $10~\mu A$, for different setpoints of the input voltage.

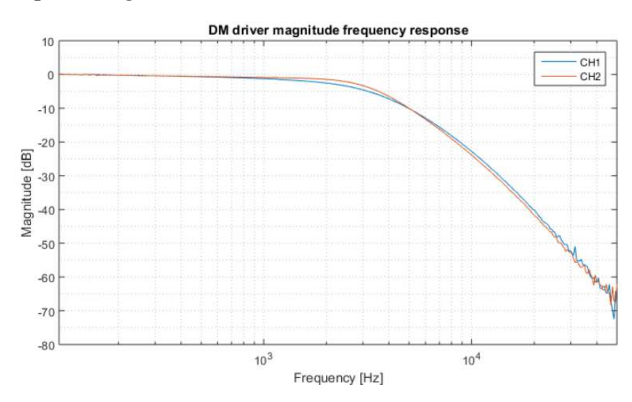


Figure 18: normalized small-signal TAA magnitude frequency response from input voltage to output load current

Figure 19: output load current noise spectral density of the TAA, for a 1V and 2.5V DC input voltage setpoint

The main driver for the development of the PWM driver boards is the low power dissipation, which allows the electronics box to be stowed in the shadow of the M2-unit on top of the spider structure without any additional cooling. Figure 20 shows the heat dissipation of the driver board with 210 operational channels with the same load current under static excitation. Under nominal operational conditions the UH2.2 ASM is anticipated to maximally require an average current of 60mA per actuator, which leads to an overall dissipation of less than 20Watts for the drive electronics for all the 210 channels (see Figure 20). This meets the requirements for the allowable power-dissipation at the top-end of the spider structure of the UH2.2 telescope.

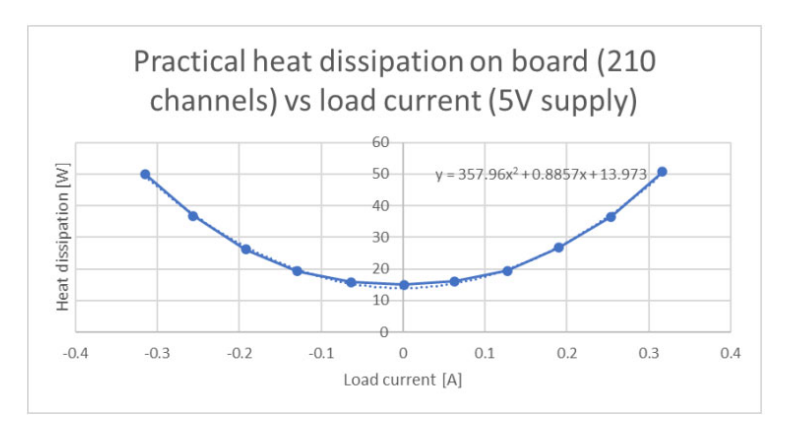


Figure 20: Total heat dissipation in the amplifier circuits as a function of load current, in case all 210 channels are commanded to generate the same load current.

Closed-loop end-to-end testing was done by hooking up the drive electronics to a 57-actuator DM previously built by TNO (Figure 21). The actuators of this DM are largely similar to the ones of the UH2.2 ASM. The displacement of the DM actuators is measured directly using six capacitive sensors that close to the mirror surface. The setup also uses the actual cable harness that will connect the driver box to the UH2.2 ASM to ensure that electronically everything is representative for the final situation on the telescope. The signals from the cap-sensors are fed-back to the real-time control computer, at which a feedback controller is tuned.

Figure 22 shows the resulting closed loop frequency responses, achieving a 150Hz sensitivity bandwidth (-3dB), and a 400Hz process sensitivity bandwidth (-3dB), which are well within the requirements.

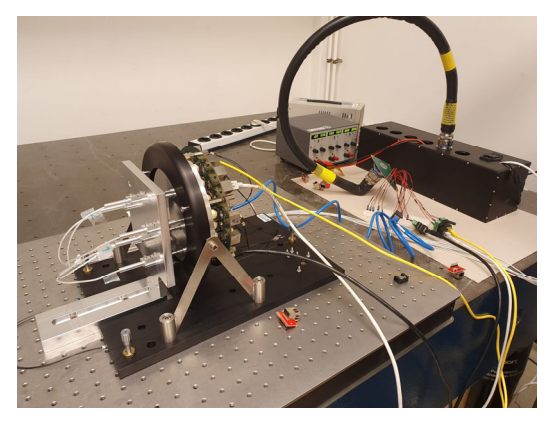


Figure 21: Electronics closed-loop end-to-end testing

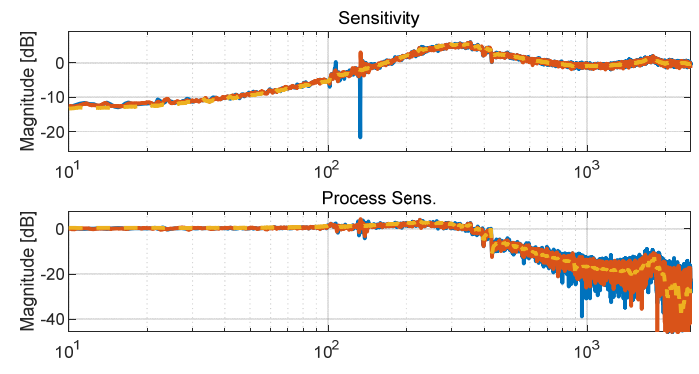


Figure 22: Closed loop sensitivity bode diagram (top) and the closed loop Process sensitivity (bottom) as measured.

CONCLUSIONS

The assembly and integration of the ASM is progressing well. All mechanical components for the ASM have been manufactured, fit checked and functionally tested. The drive electronics and digital interface were manufactured and closed-loop end-to-end tested. Detailed procedures for initial shaping of the facesheet during integration are currently being defined. The delivery of the facesheet itself around Q4 of 2022 will mark the start of the final ASM integration.

REFERENCES

- [1] Wouter Jonker, Stefan Kuiper, Jan Nijenhuis, Bert Dekker, Arjo Bos, Emiel van de Ven, Mark Chun, Hans Priem, Mathieu Breukers, "Design and MAIT status of the UH2.2 adaptive secondary mirror," Proc. SPIE 11451, Advances in Optical and Mechanical Technologies for Telescopes and Instrumentation IV, 114510O (13 December 2020); https://doi.org/10.1117/12.2561586
- [2] Mark Chun, Christoph Baranec, Olivier Lai, Jessica Lu, Stefan Kuiper, Wouter Jonker, Matt Maniscalco, "A new adaptive secondary for astronomy on the University of Hawaii 2.2-meter telescope," Proc. SPIE 11448, Adaptive Optics Systems VII, 1144852 (2020)
- [3] Stefan Kuiper, Mark Chun, Wouter Jonker, Matthew Maniscalco, Olivier Lai, Jessica Lu, "Performance analysis of the adaptive secondary mirror for the UH2.2 telescope," Proc. SPIE 11448, Adaptive Optics Systems VII, 11448229 (2020)
- [4] Rachel Bowens-Rubin, Philip Hinz, Wouter Jonker, Stefan Kuiper, Cesar Laguna, Matthew Maniscalco, "Performance of Large Format-Deformable Mirror Constructed with TNO Variable-Reluctance Actuators," Proc. SPIE 11448, Adaptive Optics Systems VII, 11448234 (2020)
- [5] Wouter Jonker, Stefan Kuiper, Fred Kamphues, Paul-Alexander Vogel, Anh-Tuan Vu, Constantin Meinders, Rik ter Horst, Thomas Arnold, "Hot forming of a large deformable mirror facesheet," Proc. SPIE 12188 (2022)